Microphysical Properties of Slow-Falling and Fast-Falling Ice Pellets Formed by Freezing Associated with Evaporative Cooling

NOBUHIRO NAGUMO

Meteorological Research Institute, Japan Meteorological Agency, Tsukuba, Ibaraki, Japan

YASUSHI FUJIYOSHI

Institute of Low Temperature Science, Hokkaido University, Sapporo, Hokkaido, Japan

(Manuscript received 6 February 2015, in final form 18 August 2015)

ABSTRACT

This paper describes a numerical and observational study focused on ice-pellet formation and microphysical properties near 0°C from an ice-pellet-dominated storm associated with an unusually warm and dry atmosphere on 10 April 2005, in Sapporo, Japan. A one-dimensional numerical model simulation indicated that precipitation particle temperatures were sensitive to environmental temperature and relative humidity and close to the wet-bulb temperature. The simulation demonstrated that completely melted snowflakes could refreeze by evaporative cooling. Moreover, initial freezing could be explained by contact ice nucleation at the height of the minimum wet-bulb temperature.

Observations using a 2D video distrometer (2DVD) indicated that ice pellets exhibited two modes of fall velocities at surface temperatures near 0°C during the same time period: slow falling and fast falling. The slow-falling ice pellets exhibited a velocity similar to the average terminal velocity of hail, whereas the velocities of the fast-falling ice pellets were closer to those of raindrops. Surface roundness and fracturing characteristics of ice pellets suggest that slow-falling ice pellets froze rapidly and uniformly in a relatively cold dry layer with a wet-bulb temperature near −4°C. In contrast, the fast-falling ice pellets exhibited the properties of ice particles with a wet smooth surface, suggesting that they froze slowly in a relatively warm layer by contacting ice crystals or splinters generated by preceding slow-falling ice pellets.

1. Introduction

Freezing rain is considered to be a hazardous weather condition, particularly in the southeastern parts of Canada, northeastern parts of the United States, and parts of East Asia (Cortinas 2000; Cortinas et al. 2004; Matsushita and Nishino 2008; Gao et al. 2013). Supercooled droplets freeze immediately upon contact with a surface at subfreezing temperatures, while ice pellets form when supercooled droplets freeze in midair (e.g., Brooks 1920; Stewart and King 1987; Crawford and Stewart 1995; Hanesiak and Stewart 1995; Stewart and Crawford 1995). Whether supercooled raindrops freeze in midair or not can determine the impact on extensive electric power outages and hazardous road conditions.

Many laboratory experiments have been conducted to investigate the freezing process of supercooled liquid drops (e.g., Blanchard 1957; Brownscombe and Thorndike 1968; Dye and Hobbs 1968; Takahashi and Yamashita 1969, 1970; Spengler and Gokhale 1972; Takahashi 1975). However, few studies have investigated the physical properties of ice pellets and freezing rain occurring in nature (Gibson and Stewart 2007; Gibson et al. 2009; Zhang et al. 2011). Even during the Canadian Atlantic Storms Program (CASP) field project, few data were collected related to the microphysical properties (i.e., shapes, sizes, and fall velocities) of ice pellets (Crawford and Stewart 1995).

In Japan, both ice pellets and freezing rain events are difficult to observe, because they are typically short lived and occur primarily in mountainous regions. However, on 10 April 2005, ice pellets fell for an extended period of time (10 h) in the area of Sapporo, Hokkaido. We

Corresponding author address: Nobuhiro Nagumo, Dept. of Meteorological Satellite and Observation System Research, Meteorological Research Institute, 1-1, Nagamine, Tsukuba, Ibaraki 305-0052, Japan.
E-mail: nagumo@mri-jma.go.jp

DOI: 10.1175/MWR-D-15-0054.1

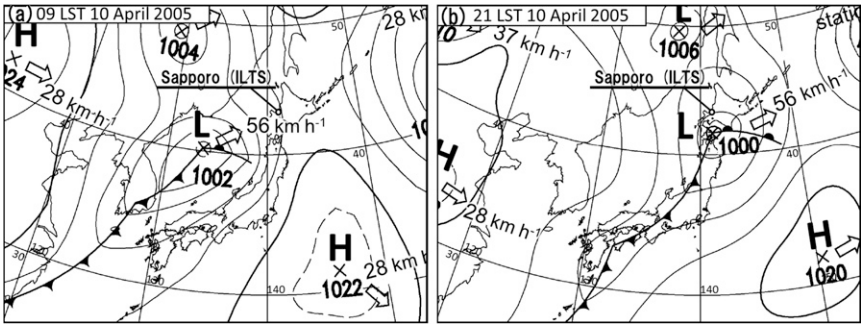

FIG. 1. Surface weather maps at (a) 0900 and (b) 1800 LST 10 Apr 2005. The location of the ILTS laboratory at Hokkaido University in Sapporo is annotated.

observed the microphysical properties of these ice pellets using a 2D video distrometer (2DVD; Schönhuber et al. 2007, 2008). This event involved unusually warm surface temperatures ranging from +1.6° to +2.7°C. The maximum of +2.7°C was quite high compared to previous cases (Cortinas et al. 2004), except that described by Kumjian and Schenkman (2014) (+14°C). Moreover, nearly a century had passed since the last record of an ice-pellet event in the Sapporo area (Matsukawa 1923).

In this paper, we present and discuss new findings regarding the microphysical properties of ice pellets and their underlying formation processes associated with evaporative cooling, based on 2DVD data and one-dimensional numerical simulations.

2. Synoptic conditions and radar echo structure

Ice pellets were observed approximately between 0800 and 1800 LST (UTC + 9 h) at the Institute of Low Temperature Science (ILTS), Hokkaido University, on 10 April 2005. Surface weather maps from the Japan Meteorological Agency (JMA) for 0900 and 1800 LST indicate that a low pressure system moved from southwest to northeast at a speed of 56 km h^{-1} (Fig. 1). ILTS was on the northeastern side of the surface warm front at 0900 LST. The warm front was passing through to the south of ILTS by 1800 LST. During this period, a stratiform radar echo moved eastward over ILTS (Fig. 2).

Figure 3 depicts vertical profiles of air temperature, dewpoint temperature, relative humidity with respect to liquid water and ice, and wind speed and direction at 0900 LST at the Sapporo District Meteorological Observatory (SDMO) of JMA, located 2 km south of ILTS. A deep warm layer was present from 0.7 to 2.3 km above ground level (AGL), with air temperatures >0°C, above a strong temperature inversion at 0.6 km. The maximum temperature within the layer (+3.6°C) was observed at 1.1 km. Below the inversion, a thin cold layer was present from 0.3 to 0.7 km, with air temperatures <0°C and a minimum temperature of −2.5°C at 0.6 km. An isothermal layer at approximately 0°C was observed in the upper part

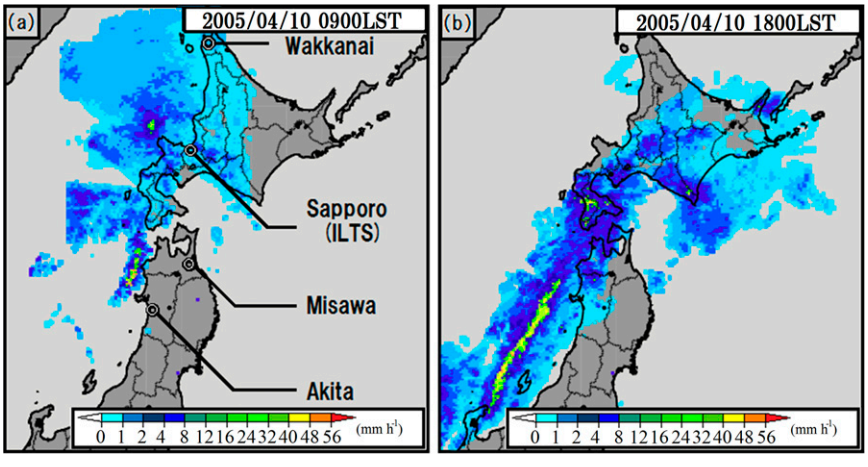

FIG. 2. Horizontal distribution of precipitation rates derived from the JMA radar at (a) 0900 and (b) 1800 LST 10 Apr 2005.

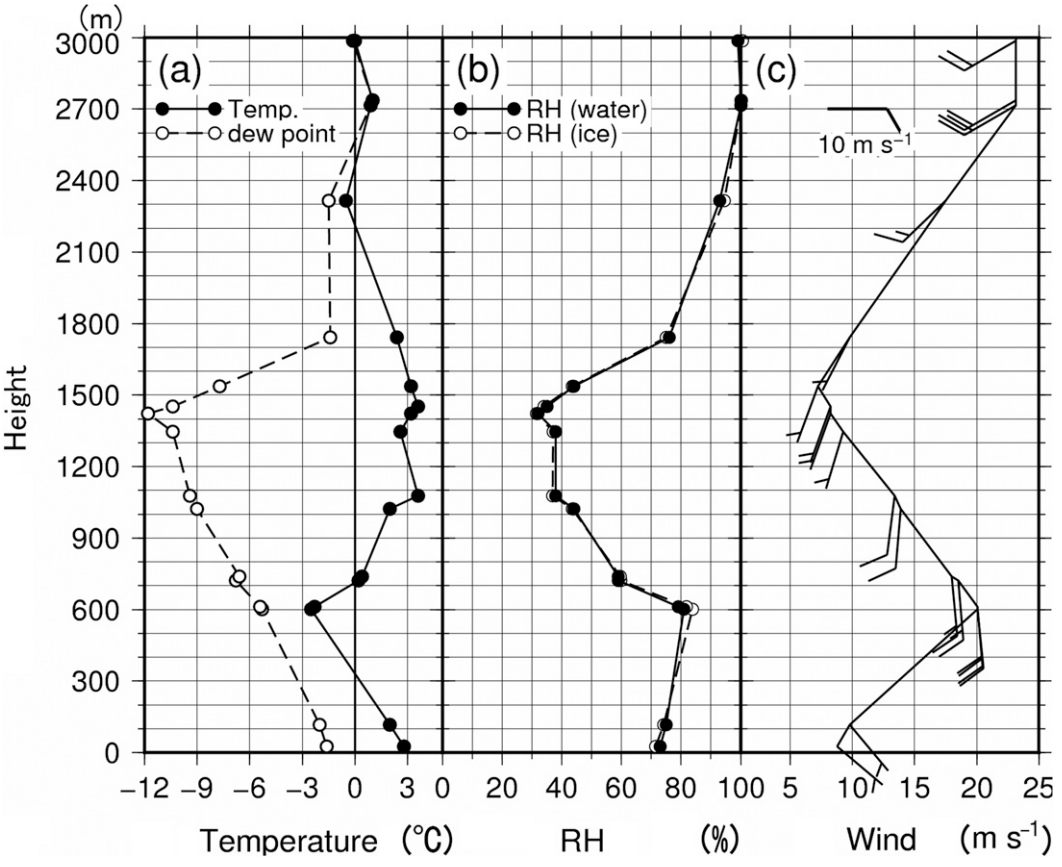

FIG. 3. Vertical profiles of (a) temperature (air temperature denoted by the solid line and dewpoint temperature denoted by the dashed line), (b) relative humidity, and (c) wind speed and wind direction observed at SDMO at 0900 LST (0000 UTC) 10 Apr 2005. Heights are in m AGL.

of the melting layer between 2.3 and 3.0 km. Subzero temperatures were observed above the isothermal layer (not shown). The relative humidity was very low in the warm layer from 0.7 to 1.8 km (Fig. 3b) with a minimum of 32% at 1.4 km. The warm and very dry air from 0.6 to 1.8 km was associated with a southerly wind (Fig. 3c).

Figure 4 depicts a latitude–height cross section of upper-air sounding data from four stations (i.e., Wakkanai, Sapporo, Misawa, and Akita in Fig. 2a). All four stations indicated a dry and warm layer from 1 to 2 km AGL. Specifically, Akita and Misawa, where no surface precipitation was observed, exhibited their minimum relative humidity (10%) in the southerly wind layer, clearly indicating that the warm and dry air was advected from the south to the Sapporo area above the cold air and southeasterly wind layer. A time–height cross section of the radar reflectivity factor over the Sapporo area was made using a series of volume scan data from the New Chitose Airport C-band plan position indicator (PPI) radar located 40 km southeast of ILTS. The radar reflectivity data, averaged between 315° and 325° in azimuthal direction, are plotted in Fig. 5. A bright band (melting layer) is apparent from 2.5 to 3 km between 0800 and 1700 LST. The lower boundary of the bright band (2.5 km) was significantly higher than the bottom of the >0°C layer (0.7 km) at 0900 LST (Fig. 3), indicating that the observed ice

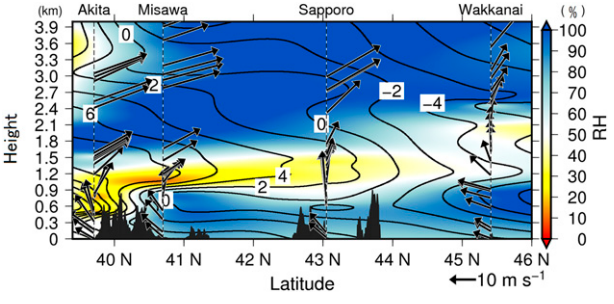

FIG. 4. Latitude–height cross section of air temperature (black contours) and relative humidity (color shade) at 0900 LST 10 Apr 2005, composited using observed data at four upper-air sounding stations located between 39° and 46°N. Air temperature is in °C and relative humidity is in %.

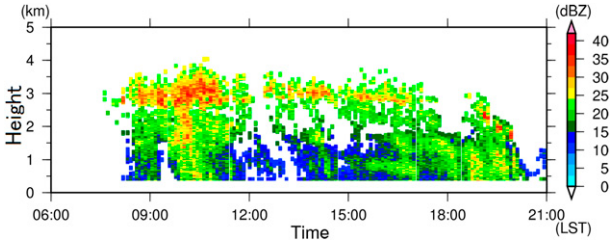

FIG. 5. Time–height cross section of the radar reflectivity factor over Sapporo on 10 Apr 2005 (LST). Heights are in km AGL.

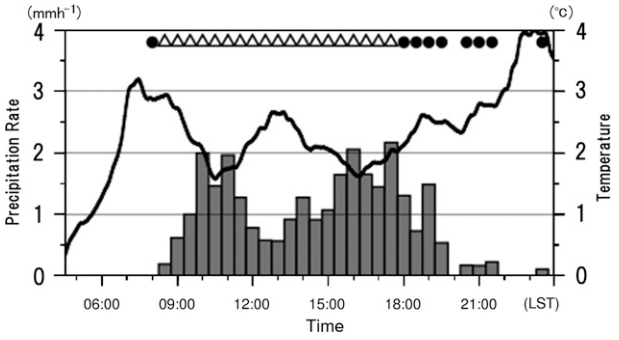

FIG. 6. Temporal evolution of precipitation rate (bars) and surface air temperature (solid line) with observed precipitation types on 10 Apr 2005. Black circles denote raindrops, and white triangles denote ice pellets. All data were obtained at ILTS.

pellets formed from completely melted snowflakes in a warm but very dry layer at this time.

3. Surface observations

Figure 6 illustrates how surface air temperature, precipitation rate, and precipitation type (i.e., rain or ice pellet) changed with time at ILTS. Surface air temperature (2 m AGL) was measured each minute using a digital thermometer (HOBO H8Pro). Precipitation rate was measured using a weighing precipitation gauge every 3 s. Precipitation type was determined from both occasional human observations and continuous 2DVD observation. Other meteorological components were observed every 10 min at SDMO.

Raindrops began to fall at 0800 LST and soon turned to ice pellets. These pellets lasted for 10 h before turning to rain after 1800 LST. The ice pellet period at ILTS coincided with the presence of a bright band aloft (Fig. 5). Although surface air temperature varied with precipitation rate, it remained above 0°C (between +1.6° and +2.7°C) throughout the ice pellet period. The surface relative humidity was 70%–90% throughout the event (not shown), which was more moist than the dry air aloft at 0900 LST in Fig. 3.

Figure 7 illustrates a horizontal distribution of mean surface air temperature between 0900 and 1800 LST and precipitation types reported at JMA surface observatories during this event. The mean air temperature at locations where ice pellets were reported ranged from −1° to +1°C. Only snow was observed where both surface and upper-air temperatures were below 0°C (Wakkanai).

Figure 8 presents representative close-up photographs of observed ice pellets. Some ice pellets exhibited no particular visual features on their surface; we classified these pellets as spherical (not shown) or nearly spherical (Fig. 8a). Other pellets exhibited interesting surface features. The majority of them had bulged surfaces (Figs. 8b–i), with one or more protrusions that were typically less than one-quarter of the particle diameter. Some of these protrusions were stumpy bulges (Figs. 8b–d), whereas others were sharp bulges (Figs. 8e–i). Although we were not able to see spicule ice pellets from these photographs, which typically exhibit an ice spike extending for more than one-quarter of the particle diameter, the 2DVD detected a small number of spicule ice pellets, as will be discussed below. Fractured ice pellets were often observed (Figs. 8e–j); some exhibited voids (Fig. 8e), cracks (Fig. 8f), a characteristic flat section with voids (Figs. 8g,h), a partially broken surface (Fig. 8i), or a sharp cut surface at a junction with other ice pellets (Fig. 8j). Fused (Fig. 8k) and aggregated

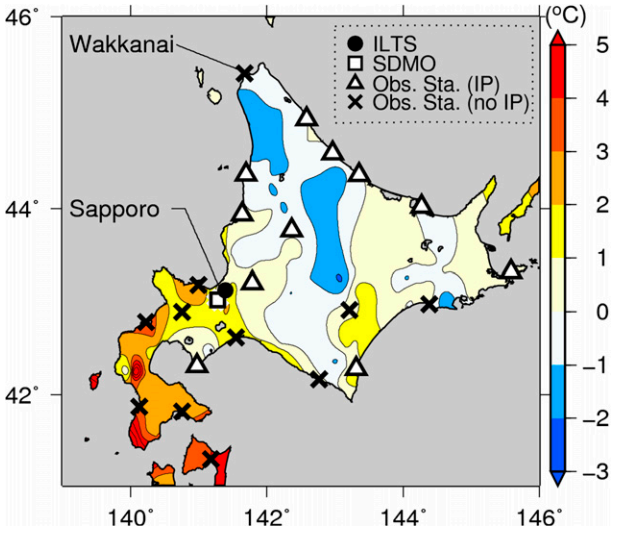

FIG. 7. Horizontal distribution of mean surface air temperatures between 0900 and 1800 LST 10 Apr 2005 at the JMA observatories, where precipitation types were also recorded. The black circle indicates the location of ILTS; the white square indicates the location of SDMO. Triangles indicate stations that observed ice pellets (IPs) during the time period of interest; crosses indicate stations that did not.

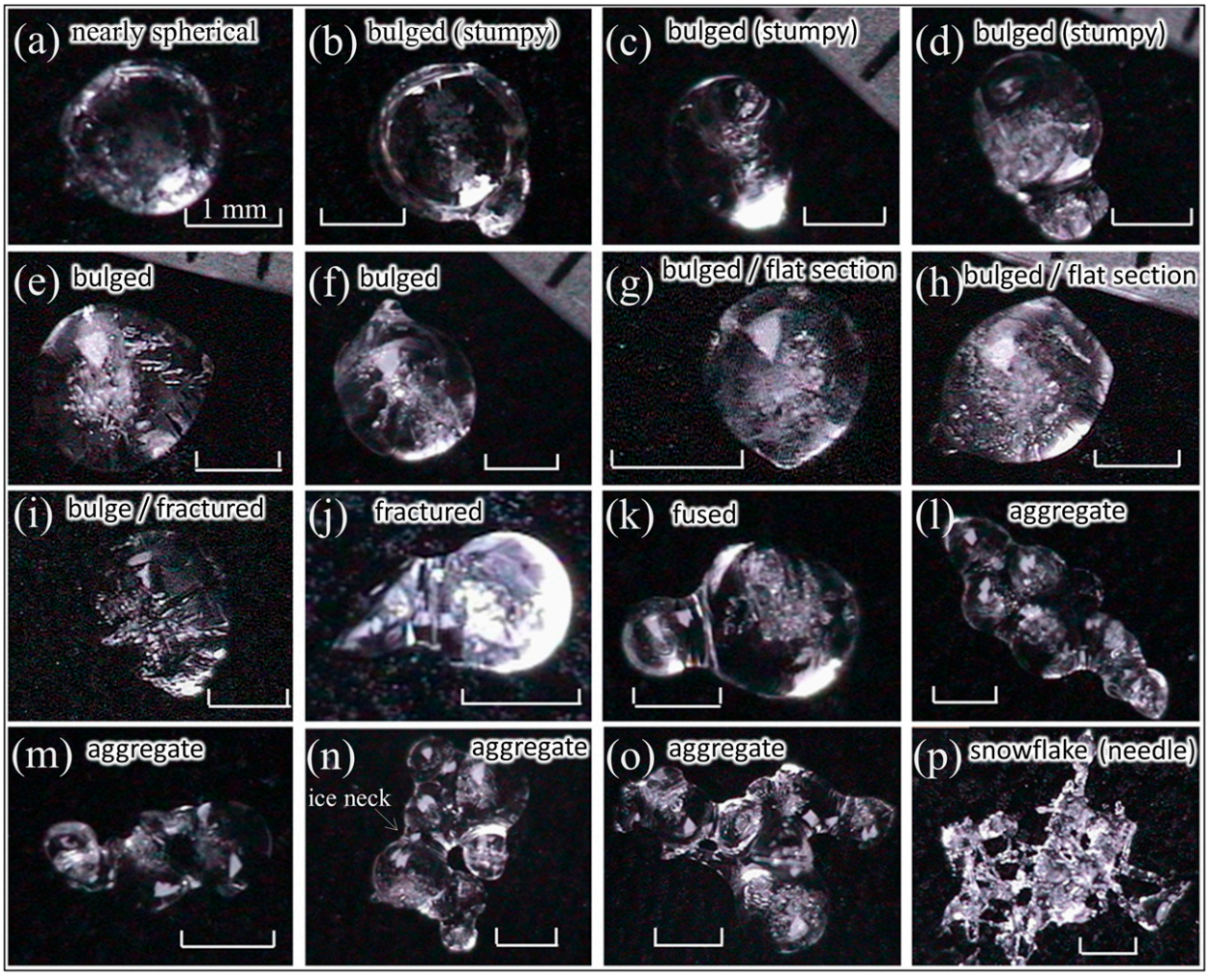

FIG. 8. Photographs of (a)–(o) ice pellets taken from 1400 to 1500 LST 10 Apr 2005, and (p) the only snowflake found during this period (representatives of 39 total photographs).

(Figs. 8l–o) ice pellets were observed occasionally. Aggregated ice pellets had multiple (more than five) particles connected by well-defined ice necks, whereas the bonding regions of fused ice pellets appeared to blend together into a single mass of ice. Most of the particles in the aggregated ice pellets were similar in size, as reported by Stewart and Crawford (1995). The aggregated ice pellets monitored by 2DVD tended to exhibit longitudinal orientation (not shown), suggesting that aggregation might be promoted at the leading edge.

Only one snowflake composed of needle snow crystals was found in the collection of photographs taken from 1400 to 1500 LST (Fig. 8p). Note that some pellets melted slightly, because these photographs were taken several seconds after collection.

The fall velocities and volume-equivalent diameters (hereafter diameter) of ice pellets were measured using 2DVD. These diameters are calculated from 2DVD scan-line heights and widths as follows (Schönhuber et al. 2008). The scan lines divide a particle into several slices. These slices are assumed to form elliptical cylinders from two directions of lines. Summing up all the slices, the particle volume is obtained, which can be translated into its diameter.

The resolution of the measured diameter is better than 0.19 mm, and the variation of error for the fall velocity measurements is better than 4% for velocities below $10\,m\,s^{-1}$ (Schönhuber et al. 2007). In this study, particle diameters exceeding 0.5 mm and particle speeds less than $10\,m\,s^{-1}$ were considered for determination of individual particle shapes. Furthermore, erroneous data arise from mismatches in detected particles when two or more particles pass the measurement area coincidentally and exhibit unusually oblate or prolate shapes. These erroneous data (~10%) were excluded manually by visual inspection of the particle images.

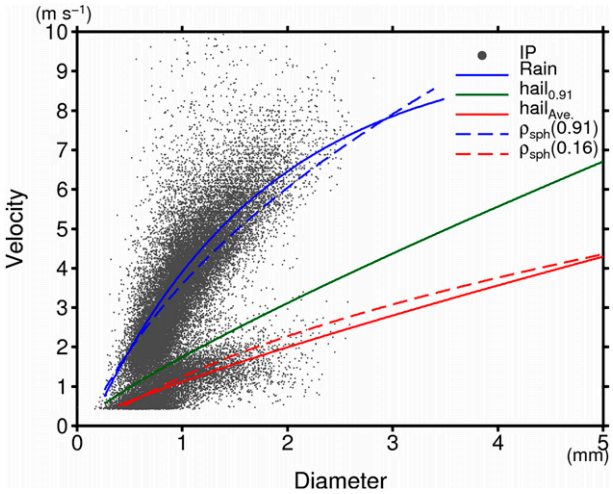

FIG. 9. Relationship between fall velocity and diameter of IPs observed from 0900 to 1000 LST. The solid blue line indicates velocity–diameter relationships for raindrops (Atlas et al. 1973), the solid green line indicates hailstones with a density of 0.91 g cm^{-3}, and the solid red line indicates the average density of hailstones (0.44 g cm^{-3}) (Knight and Heymsfield 1983). The dashed blue line indicates terminal fall velocities for smooth ice spheres with densities of 0.91 g cm^{-3}, and the dashed red line indicates those for smooth ice spheres with densities of 0.16 g cm^{-3} (Mikhailov and Silva Freire 2013). The fall velocity relationships for hail are extrapolated to particles smaller than 5 mm in size that are typically not considered to be hail.

Figure 9 plots the fall velocities of ice pellets against their diameters. Two modes of ice particle terminal velocity are evident: fast-falling and slow-falling pellets. The velocities of fast-falling pellets were very close to the raindrop terminal velocity (Atlas et al. 1973). The velocities of slow-falling pellets were close to a terminal velocity of average-density (0.44 g cm^{-3}) hailstones (Knight and Heymsfield 1983). In section 4b, reasons for classifying the two modes of fall velocity are discussed in detail from the viewpoint of ice pellet geometrical properties in 2DVD data and in comparison with previous studies on precipitation particle microphysics.

4. Discussion

a. *Validation of freezing by evaporative cooling*

1) NUMERICAL SIMULATIONS

One-dimensional simulations were performed to investigate the possibility of refreezing of raindrops under the observed environmental conditions. The simulation framework was based on Matsuo and Sasyo (1981a,b). Since we focused on the temperature of precipitation particles T_p just before freezing, we assumed that the melted particles remain liquid during cooling even when their temperatures were below 0°C. To consider vertical environmental conditions, linearly interpolated air temperature and relative humidity profiles (Fig. 3) were used for the model simulations. In Matsuo and Sasyo (1981a,b), the heat transported from the surrounding air to a snowflake is given as

$$H = \varepsilon H' = 4\pi\varepsilon R(aK\Delta T + bL_V D\Delta\sigma), \qquad (1)$$

where ε is determined experimentally and depends on snowflake properties (e.g., porosity and sphericity). Here, R is the particle radius, $a(b)$ is the ventilation coefficient for heat (water vapor diffusion), K is the thermal conductivity, L_V is the latent heat of vaporization of water, D is water vapor molecular diffusivity, ΔT is the temperature difference between a precipitation particle and the environment, and $\Delta\sigma$ is the difference between the water vapor density of environment and equilibrium water vapor density of a particle. The particle temperature was calculated using Eq. (1) by iteration considering the fall velocity and environmental conditions with thermal relaxation times of several seconds (Watts 1971). The particle size change was calculated from the balance equation between the heat transport and latent heat associated with a phase change of the precipitation particle. For raindrops, the equation is

$$4\pi R(aK\Delta T + bL_V D\Delta\sigma)\Delta t = -4\pi R^2\rho_p L_f \Delta R. \qquad (2)$$

Here, ρ_p is the particle density, L_f is the latent heat of melting, and ΔR is the particle size change over a time step of Δt. The discretized ΔR was calculated using a Δt of 0.03 s. All precipitation particles were assumed to start as dry spherical snowflakes with 0.04, 0.02, or 0.005 g cm^{-3} density. The initial diameter of dry snowflakes varied in 0.5-mm increments from 1.0 to 10.0 mm. The terminal velocity before and during melting was calculated from the balance between drag and gravity, whereas that after melting was based on the raindrop terminal velocity of Atlas et al. (1973). For melting particles, the densities were calculated from particle size and mass while tracking water and ice mass separately. In addition, we did not consider any feedback from the environment, such as cooling and humidification by vaporization, because the observed sounding data used in the simulation already included such factors.

Figure 10 presents the results of simulations for snowflakes with initial diameters of 10.0 and 5.0 mm and density of 0.02 g cm^{-3}. Table 1 lists the results for other particles. All of the simulations started at a height of 2150 m, where the air temperature is 0°C, just above the melting layer. The snowflake temperatures immediately decrease to below 0°C as a result of evaporative cooling

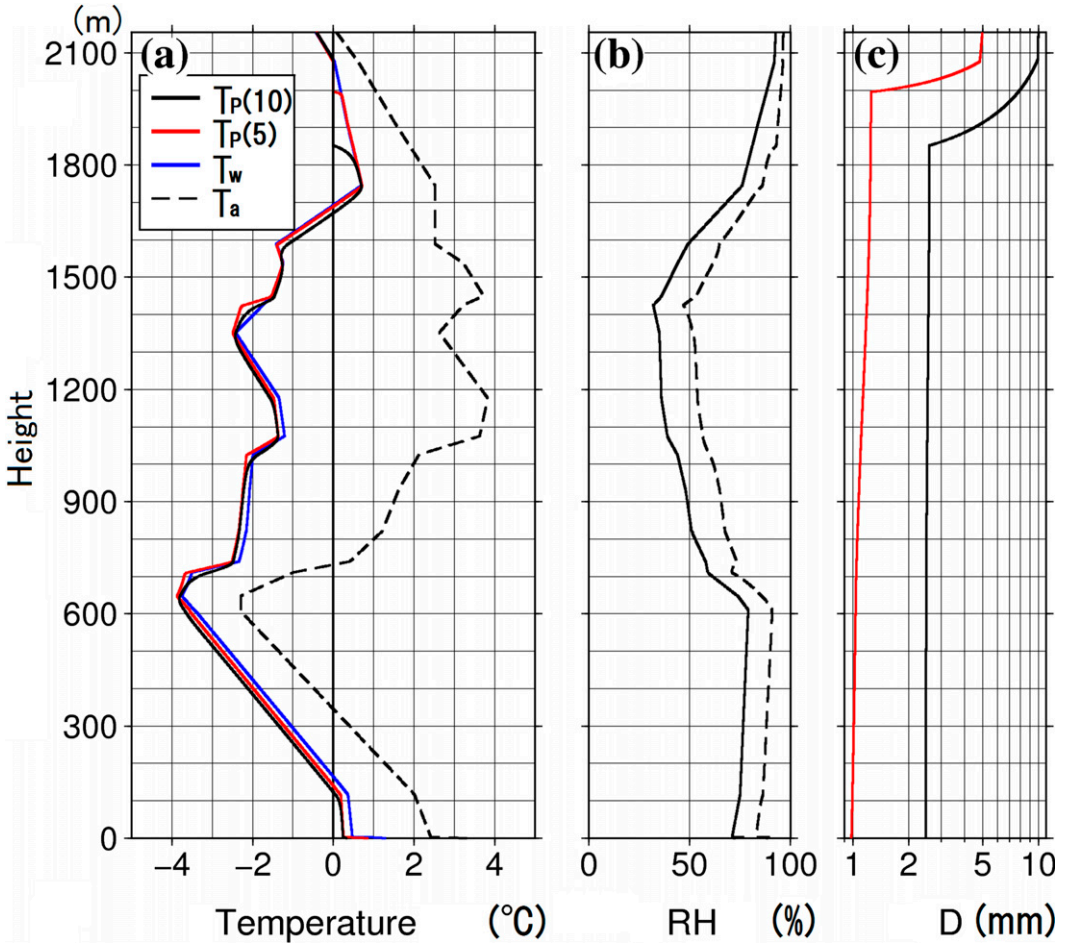

FIG. 10. Vertical profiles of environmental and simulated particle conditions. (a) Particle temperature T_p, air temperature T_a, and wet-bulb temperature T_w based on sounding data in Fig. 3. (b) Relative humidity profile with respect to liquid (solid line) and ice (dashed line). (c) Simulated particle diameter at each vertical level. Black lines denote initial particle diameters of 10.0 mm, and red lines denote those of 5.0 mm.

just below the model top (Fig. 10a). The snowflakes then begin to melt at 2100 m (Figs. 10a,c). The snowflakes with an initial size of 10.0 mm melt completely at 1850 m, and those with an initial size of 5.0 mm melt completely at 2000 m. Only large dry snowflakes over 10.0 mm with a density of 0.04 g cm^{-3} remain unmelted (Table 1). Small dry snowflakes (e.g., diameter $<$ 3.8 mm, density = 0.02 g cm^{-3}) disappear primarily through sublimation. The snowflakes with an initial diameter of 10.0 mm and a density of 0.02 g cm^{-3} turn into raindrops with a diameter of 2.5 mm at ground level. This diameter is close to the largest single ice pellets observed using the 2DVD during this event, indicating that the initial values used in this simulation are consistent with surface observations.

After complete melting, the temperatures of all precipitation particles exhibit almost the same profile below 1850 m and are less than 0°C from 1680 to 120 m. This simulation indicated that melted particles were able to remain supercooled as a result of evaporative cooling, with temperatures very close to the wet-bulb temperature (blue line in Fig. 10a) (Martinez 1994; Bohren and Albrecht 1998). For a snowflake with an initial diameter of 10.0 mm and a density of 0.02 g cm^{-3}, the layer where $T_p > 0$°C (and thus melting occurred) was only 407 m thick with a maximum particle temperature of +0.68°C. The layer where $T_p < 0$°C was 1552 m thick with a minimum particle temperature of −3.9°C.

2) DIAGNOSTIC EVALUATION

A typical ice-pellet event is characterized by a melting layer aloft ($T > 0$°C) and a thick refreezing layer ($T < 0$°C) adjacent to the surface (Stewart and King 1987). Typical formation processes have been discussed for cold environments, with little impact from evaporative cooling (Stewart and Crawford 1995; Zerr 1997; Zhang et al. 2011). However, the temperature of the

TABLE 1. Results from theoretical one-dimensional model simulations. The warm (cold) layer in this table corresponds to the layer in which particle temperature T_p is more than or equal to (below) 0°C, not a conventional melting (freezing) layer from environmental temperature. Here, "sub." indicates "sublimated" and NM indicates "not melted" at ground.

		D at top (mm)									
		1.0	2.0	3.0	4.0	5.0	6.0	7.0	8.0	9.0	10.0
ρ_i 0.04 g cm^{-3} heavy	Warm-layer depth (m)	—	360	398	400	404	396	397	402	405	—
	Warm-layer max temp (°C)	—	0.63	0.7	0.7	0.69	0.65	0.64	0.59	0.32	—
	Cold-layer depth (m)	—	—	1550	1548	1552	1562	1560	1554	1554	—
	Cold-layer min temp (°C)	—	—	−3.9	−3.8	−3.8	−3.9	−3.9	−3.8	−3.8	—
	Melted height (m)	2075	2025	2010	1964	1919	1870	1824	1780	1736	—
	Sublimation height (m)	1894	1276	—	—	—	—	—	—	—	—
	Diameter at ground (mm)	Sub.	Sub.	0.35	0.93	1.32	1.69	2.03	2.35	2.68	NM
ρ_i 0.02 g cm^{-3} medium	Warm-layer depth (m)	—	397	399	374	395	404	393	405	397	407
	Warm-layer max temp (°C)	—	0.74	0.72	0.62	0.68	0.69	0.65	0.68	0.65	0.68
	Cold-layer depth (m)	—	—	—	1566	1552	1550	1557	1550	1560	1552
	Cold-layer min temp (°C)	—	—	—	−3.9	−3.9	−3.8	−3.9	−3.8	−3.9	−3.8
	Melting height (m)	–	2072	2052	2011	1994	1969	1934	1909	1877	1850
	Sublimation height (m)	2110	1530	941	—	—	—	—	—	—	—
	Diameter at ground (mm)	Sub.	Sub.	Sub.	0.56	0.98	1.31	1.61	1.90	2.18	2.46
ρ_i 0.005 g cm^{-3} light	Warm-layer depth (m)	—	—	—	390	394	375	400	402	396	382
	Warm-layer max temp (°C)	—	—	—	0.71	0.71	0.64	0.70	0.69	0.67	0.63
	Cold-layer depth (m)	—	—	—	—	—	—	1547	1552	1556	1567
	Cold-layer min temp (°C)	—	—	—	—	—	—	−3.9	−3.9	−3.9	−3.9
	Melting height (m)	—	—	—	2073	2068	2046	2051	2042	2028	2010
	Sublimation height (m)	2158	2129	2085	1523	1108	270	—	—	—	—
	Diameter at ground (mm)	Sub.	Sub.	Sub.	Sub.	Sub.	Sub.	0.67	0.93	1.15	1.34

refreezing layer on 10 April 2005, reaching a minimum of −2.5°C, was higher than for previously observed ice-pellet events [e.g., −10° to −6°C in Zerr (1997)]. The refreezing layer thickness of 0.4 km was also thinner than that in previous reports [e.g., 0.8–1.8 km in Zerr (1997)]. We posit that the 10 April 2005 event was strongly influenced by evaporative cooling due to extremely dry conditions, in agreement with previous studies (e.g., Hanesiak and Stewart 1995; Kumjian and Schenkman 2014).

To analyze the state of hydrometeors reaching the surface (i.e., supercooled raindrops or ice pellets), we computed melting and refreezing parameters that are defined in Zerr (1997) using the observed air temperature and wet-bulb temperature for this event. The melting (freezing) parameter is defined as multiplication of the depth (km) of a melting (refreezing) layer and a maximum (minimum) temperature (°C) found in the layer (Zerr 1997). The results are presented in Fig. 11, which also includes the results of Zerr (1997). These two parameters calculated from the observed air temperature (open square in Fig. 11) lie among those associated with freezing rain events (crosses or minus signs) reported by Zerr (1997). However, these two parameters calculated from the observed wet-bulb temperature (triangle) were found to be closer to ice-pellet events (dots) reported by Zerr (1997). Many of the cases in Zerr (1997) were relatively moist, with little impact from evaporative cooling found. Therefore, our diagnostic determination of particle type using wet-bulb temperature (i.e., considering temperature and relative humidity) seems more appropriate than using air temperature.

3) MICROPHYSICAL INTERPRETATIONS OF ICE-PELLET FORMATION

Ice-pellet formation from completely melted raindrops could have occurred most likely through freezing with contact nucleation. The observed air temperature (Fig. 3) and the simulated particle temperatures (wet-bulb temperatures) (Fig. 10) in the refreezing layer are much higher than −10°C. A larger number of aerosol particles act as ice-forming nuclei in the contact mode than in the immersion mode, especially at a temperature above −10°C, although leaf-derived nuclei, bacteria-derived nuclei, and organic residues can initiate ice at temperatures warmer than −5°C (Edwards and Evans 1971; Pruppacher and Klett 1997). Contact nuclei reduce the energy barrier required for ice formation. The freezing of water drops in contact with sand starts at −3°C and that of water drops in contact with clay particles starts at −4.5°C, with median freezing temperatures between −4° and −6°C (Gokhale and Spengler 1972; Pitter and Pruppacher 1973). Under dry conditions, residues of evaporated cloud and

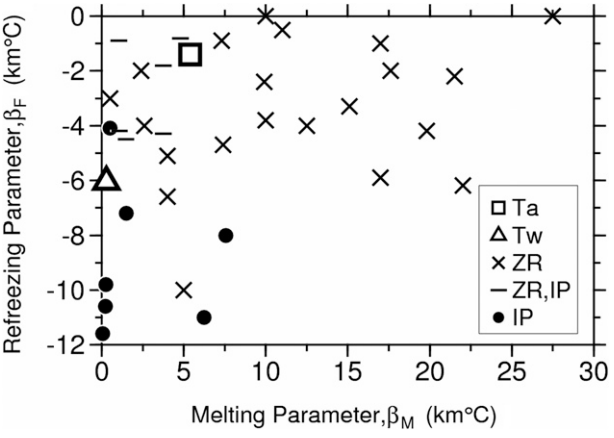

FIG. 11. Melting parameter vs refreezing parameter based on Zerr (1997). The square (T_a) denotes the parameters computed from the air temperature from a sounding at SDMO at 0900 LST. The triangle (T_w) denotes those from the simulated wet-bulb temperature. Other data points are observations presented in Zerr (1997). ZR denotes freezing rain, and IP denotes ice pellets.

precipitation particles can also serve as evaporation ice nuclei (Beard 1992). Several observational studies have also supported ice formation at warm temperatures (i.e., from −4° to −5°C) (Mossop et al. 1968; Sassen et al. 2003).

The results of simulations in Fig. 10 indicate that temperatures of precipitation particles reached the wet-bulb temperature just below the initial height level, which implies that particle temperatures are quite sensitive to changes in both temperature and relative humidity. As indicated earlier, the dry midlevel over Sapporo was advected from the south, and Sapporo was located near the edge of the precipitation region (Fig. 2). The lowest relative humidity at 0900 LST in Fig. 3 corresponded to a low mixing ratio of 1.83 g kg^{-1}, which already included the influence of humidification by the evaporation of precipitation particles. Conversely, the sounding at Misawa to the south of Sapporo, where no rain was detected, had very low relative humidity (less than 15% in Fig. 4). This value corresponds to a lower mixing ratio of 0.91 g kg^{-1}. A small difference in mixing ratio could significantly impact the relative humidity at temperatures near 0°C and thus could result in more favorable dry conditions for refreezing. Additional model simulations were performed to investigate this possibility. The simulation results for an initial particle diameter of 10.0 mm and a density of 0.02 g cm^{-3} are presented in Fig. 12 for decreases in relative humidity of 15% and 30% between 600 and 1700 m compared to Fig. 10. Relative humidity decreases of 15%–30% resulted in decreases of 1°–2°C in particle temperature, with a minimum temperature of less than −4 to −5°C at altitudes between 600 and 1700 m. Although this temperature cannot entirely explain immersion freezing, the possibility of freezing by contact nucleation extends to a thicker layer.

Other processes of contact with ice crystals, ice splinters, or other ice pellets are required to explain the fact that almost all observed particles were ice pellets. The number concentration of ice-forming nuclei at −5°C has been reported to be within a range of 0.01–0.1 L^{-1} (Beard 1992), and this activity decreases with increasing temperature (Berezinski et al. 1988). In this warm event, the 1-h (0900–0959 LST) average number concentration of ice pellets with diameters exceeding 0.05 mm was 0.3 L^{-1}, and maximum number concentrations of 1.1 L^{-1} were recorded at 1100, 1300, and 1500 LST using 2DVD. These ice pellet concentrations were much higher than the reported number concentrations of ice-forming nuclei. Some studies suggest ice multiplication in the freezing layer as causing the increase in differential radar reflectivity Z_{DR} (Kumjian et al. 2013; Ryzhkov et al. 2011). Stewart and Crawford (1995) observed needlelike crystals in 75% of their ice pellet cases. Ice multiplication in a freezing layer is suggested to be promoted by contact between supercooled raindrops and ice splinters ejected from fractured ice particles (Pruppacher and Schlamp 1975). Once a number of ice splinters and small crystals have formed in the atmosphere, it is possible for a large number of unfrozen supercooled drops to freeze below the wet-bulb temperature of −2°C (Gokhale and Spengler 1972). Then, all of the altitudes above 400 m in this event should be favorable for the formation of ice pellets (Fig. 10a). Ice supersaturation with respect to particle temperature may also encourage contact freezing by promoting the growth of ice crystals or splinters, although the simulated ice supersaturation layer was very shallow, at around 600 m (Fig. 12b).

b. *Relationship between ice pellet fall velocity and geometry*

1) CLASSIFICATION OF ICE-PELLET GEOMETRICAL CHARACTERISTICS

Figure 13 presents representative ice-pellet images recorded using 2DVD during this event. The total number of large ice particles was 12 405. Similar to previous studies (e.g., Takahashi 1975; Gibson and Stewart 2007; Gibson et al. 2009), ice pellets were classified into seven categories: spherical, nearly spherical, bulged, spicule, irregular, fractured, and aggregated/fused pellets. Because small particles were difficult to classify, only particles exceeding 1.5 mm in diameter were considered (Table 2). In addition to the seven categories, raindrop-like particles with a round top and a flat bottom were classified as raindrops. Nearly spherical ice pellets were

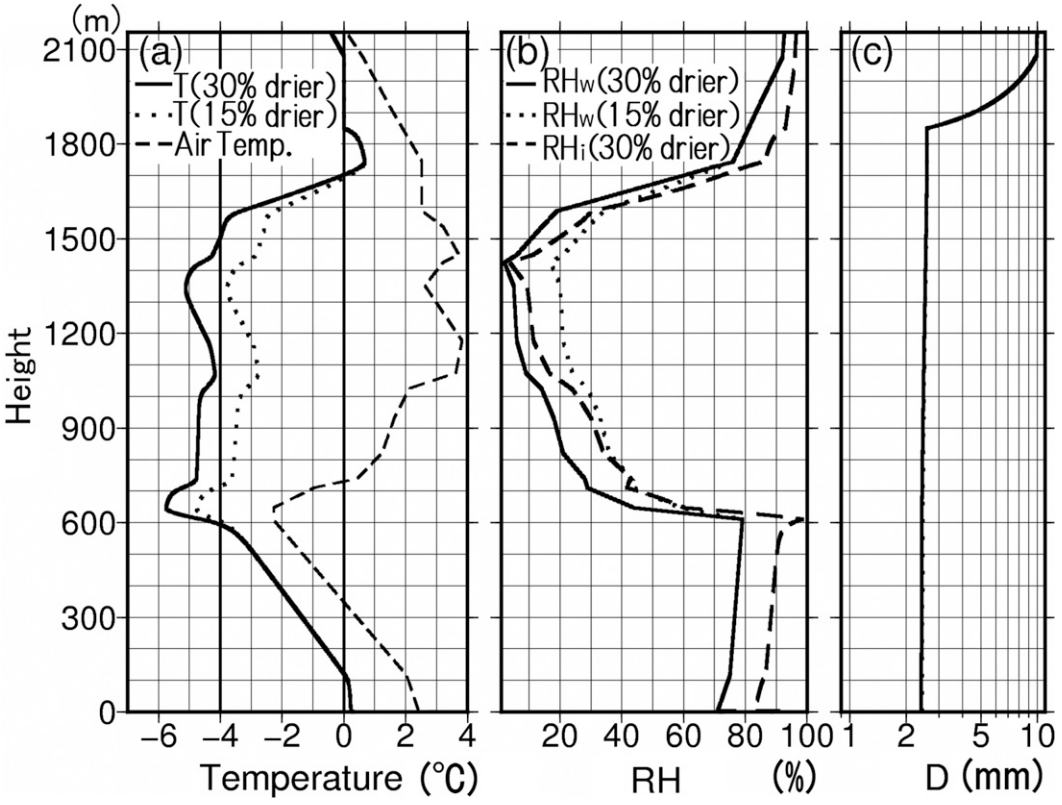

FIG. 12. Vertical profiles of simulated particles in the environments altered from Fig. 10 at 600–1700 m. (a) Particle temperature: solid line shows particle temperature with 30% drier relative humidity than in Fig. 10, dotted line shows particle temperature with 15% drier relative humidity than in Fig. 10, and dashed line denotes air temperature. (b) Relative humidity: solid line indicates 30% drier, dotted line 15% drier, and thick dashed line denotes relative humidity of ice in the 30% drier simulation. (c) Particle diameter: solid line indicates 30% drier, dotted line 15% drier. The dotted line overlaps the solid line. Initial snowflake conditions of this simulation: diameter is 10.0 mm and density is 0.02 g cm^{-3}.

defined as round particles with a slightly deformed surface not large enough to be bulges (Gibson et al. 2009).

Objective classification methods using parameters such as complexity, employed by Schmitt and Heymsfield (2014), were not applicable to ice pellets because of their simple shapes. Results in Table 2 were obtained from careful visual classifications using the 2DVD dataset. The bulged ice pellet was the most common type, comprising half of all pellets, followed by the nearly spherical type. The percentage of each category was close to that reported by Gibson et al. (2009), despite the unusually warm temperatures, except for the spicule and irregular types.

The 2DVD images were divided into fast- and slow-falling ice pellets, and large (>1.5 mm) and small (<1.0 mm) pellets. Almost all large fast-falling pellets had slightly deformed round surfaces (Fig. 13a), whereas almost all large slow-falling pellets had round surfaces (Fig. 13e). The bulged ice pellets in the fast-falling group exhibited one or more stumpy protrusions (Fig. 13b), whereas those in the slow-falling group typically had sharp protrusions (Fig. 13f). The spicule ice pellets were similar to bulged ones, except for their protrusion lengths. Furthermore, almost all fast-falling ice pellets exhibited longitudinal orientations with small canting angles (Fig. 13c), whereas all slow-falling ice pellets exhibited nearly sideway orientations (Fig. 13g), as reported by List and Schemenauer (1971). Fractured particles were rarely found in the fast-falling group, whereas the slow-falling group exhibited several types of fracture (Figs. 13h–k). Ice pellets with flat sections (Fig. 13h), jagged sections (Fig. 13i), curled sections (Fig. 13j), or broken parts (Fig. 13k) were primarily detected. Those with flat sections are exemplified in Fig. 8h, and the broken ones in Fig. 8i. These types of fractures can be considered typical shapes, as noted by Takahashi (1975). No hemispherical particles were larger than 1.5 mm, whereas some small slow-falling ice pellets were hemispherical (Fig. 13n). Ice fragments were also detected (Fig. 13o).

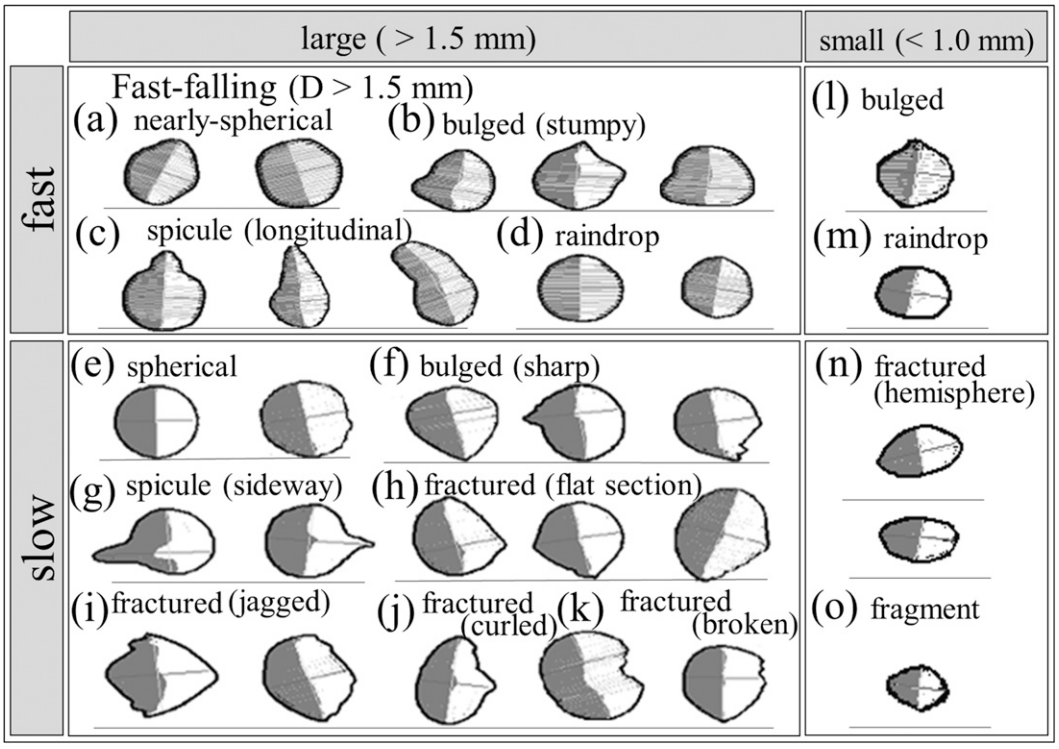

FIG. 13. IP silhouettes from 2DVD. Typical images of (a)–(d) large, fast-falling pellets; (e)–(k) large, slow-falling pellets; (l),(m) small, fast-falling pellets; and (n),(o) small, slow-falling pellets.

Figure 14 illustrates histograms of categories for both fast- and slow-falling large ice pellets. Fast-falling pellets accounted for 80% of all particles. Similar to the results presented in Table 2, the bulged pellet was the most common type in both groups (49% in the fast-falling group and 62% in the slow-falling group). Nearly spherical particles were the second most common type (40%) in the fast-falling group; however, fractured particles were the second most common type (17%) in the slow-falling group. In addition to small differences in surface roundness of ice pellets, the percentage of fractured particles was the major difference between the fast- and slow-falling groups. Aggregated and fused ice pellets were found in both groups, and their frequency of occurrence was small in this event (1.5%).

2) PROPERTIES OF ICE PELLETS DERIVED FROM FALL VELOCITIES

The bimodal distribution of fall velocities of ice pellets indicates that ice pellets with distinctively different characteristics were present. The overall velocity–diameter relationship of fast-falling particles was similar to that of

TABLE 2. Total number and frequency of occurrence of ice-pellet categories observed on 10 Apr 2005, and those reported by Gibson et al. (2009). Boldface font indicates the top two categories in each case.

	ILTS event 10 Apr 2005		Gibson et al. (2009)					
			4 Nov 2003		17 Jan 2006		16 Feb 2006	
Particle type	No.	%	No.	%	No.	%	No.	%
Bulged	**6300**	**51**	**477**	**47**	**463**	**57**	**1777**	**59.5**
Spicule	108	0.9	36	3.5	76	9.5	142	5
Fractured	422	3.4	31	3	18	2	338	11
Spherical	1057	8.5	75	7.5	12	1.5	86	3
Nearly spherical	**4025**	**32**	**296**	**29**	40	5	**493**	**16.5**
Irregular	22	0.17	57	5.5	**125**	**15.5**	109	3.5
Aggregates/fused	193	1.5	87	8.5	74	9.5	39	1.5
Rain	278	2.2	—	—	—	—	—	—

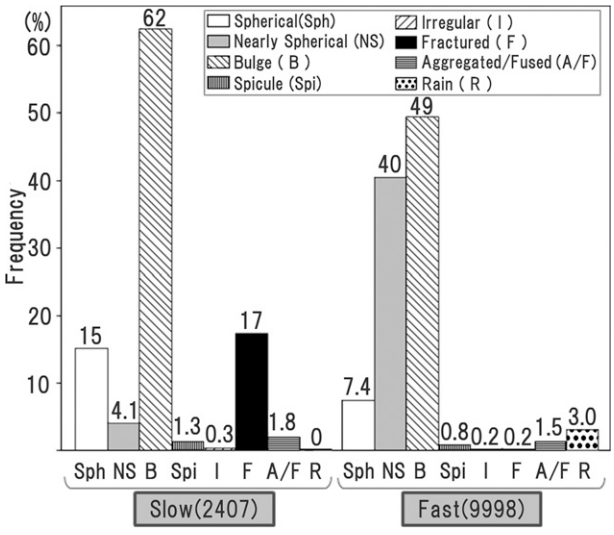

FIG. 14. Histogram of classes of fast- and slow-falling ice pellets larger than 1.5 mm in diameter, with their total numbers in parentheses.

raindrops (blue line in Fig. 9) (Atlas et al. 1973). However, smaller (larger) ice pellets tended to fall slower (faster) than raindrops. The determinant of the bimodal fall velocity was investigated by focusing on the ice-pellet densities and drag coefficient. In this section, the particles with a $V\,(\mathrm{m\,s^{-1}}) < 2D$ (mm) in Fig. 9 were considered to be slow falling.

The particle terminal velocity depends on its density and drag coefficient as

$$V = \left[\frac{4gD(\rho_p - \rho_a)}{3\rho_a C_D}\right]^{1/2}, \qquad (3)$$

where V is the terminal velocity, g is gravitational acceleration, D is particle diameter, ρ_p is particle density, ρ_a is air density, and C_D is a drag coefficient. Assuming that the particles were smooth spheres, the bulk density of the ice pellets was calculated from the fall velocity and particle diameter measured using the 2DVD. The value of C_D for smooth particles was based on Eq. (8) of Mikhailov and Silva Freire (2013). The calculated mean bulk density and standard deviation were $0.16 \pm 0.07\,\mathrm{g\,cm^{-3}}$, indicating that the ice pellets contained 75%–90% air by volume (red dashed line in Fig. 9). This extremely low density could possibly be explained by spillage of unfrozen water (Spengler and Gokhale 1972). Fractured ice pellets that were categorized in the slow-falling group exhibited evidence of water spillage from voids (Fig. 15). However, these images could not explain the slow fall velocity by density alone, because they did not indicate a large amount of air in the particles.

Another determining factor is the drag coefficient. A very tiny (microscopic scale) rough surface can have a significant impact on the drag coefficient of small particles with a low Reynolds number (Selberg and Nicholls 1968; Rasmussen and Heymsfield 1987; Heymsfield and Wright 2014). Since dry hailstones with densities of $0.91\,\mathrm{g\,cm^{-3}}$ have tiny rough surfaces and high drag coefficients (Knight and Heymsfield 1983), their terminal fall velocities are significantly lower than those of smooth ice spheres (dotted blue and green lines in Fig. 9) (Knight and Heymsfield 1983; Thériault and Stewart 2010; Kumjian et al. 2012). Most of the slow-falling particles were even slower than hailstones with densities of $0.91\,\mathrm{g\,cm^{-3}}$and close to the fall velocity of average-density ($0.44\,\mathrm{g\,cm^{-3}}$) hail (solid red line in Fig. 9) (Knight and Heymsfield 1983). These facts suggest that the slow-falling particles had very tiny rough surfaces, similar to those of dry hailstones.

Another factor that increases the drag coefficient is tumbling motion (List and Schemenauer 1971). This occurs when freezing drops coagulate (Spengler and Gokhale 1972) and turn to dry ice particles (Bringi and Chandrasekar 2001; Straka 2009; Anderson et al. 2011; Ryzhkov et al. 2011). This motion could reduce the fall velocity even more.

Fast-falling large pellets tended to fall faster than spherical ice particles with smooth surfaces and densities of $0.91\,\mathrm{g\,cm^{-3}}$ (blue dashed line in Fig. 9), suggesting that fast-falling ice pellets likely had smooth surfaces and that their interiors were possibly still liquid water.

3) FORMATION PROCESS INFERRED FROM GEOMETRICAL AND FALL VELOCITY CHARACTERISTICS

The different geometrical properties of fast- and slow-falling ice pellets observed in this study also suggest different freezing mechanisms of the two groups of ice pellets. The surfaces of the slow-falling ice pellets were typically round surfaces and some were fractured, as observed in 2DVD images (Fig. 13). Some cracks were also seen in photographs of fractured ice pellets (Fig. 15). Although the 2DVD is unable to detect cracks, Takahashi and Yamashita (1969) found that cracking is more likely to occur than fracturing. Conversely, the surfaces of the typical fast-falling ice pellets were slightly deformed without fractures. This apparent difference in surface features suggests a difference in freezing speeds, which typically depend on the degree of supercooling (Yang and Good 1966; Pruppacher 1967; Johnson and Hallett 1968; Gokhale and Lewinter 1971; Pruppacher and Klett 1997), between the two groups.

The freezing of a liquid particle starts at the outside of the particle and proceeds inward (Gokhale and Lewinter

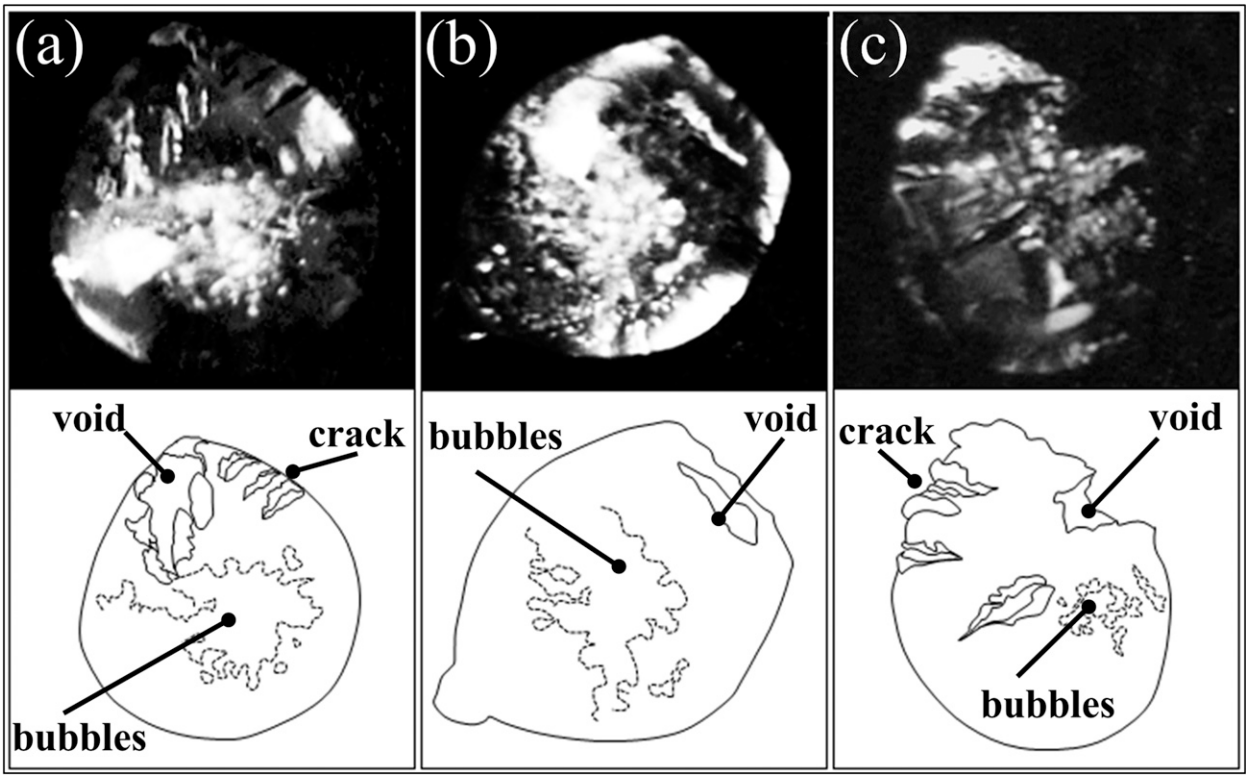

FIG. 15. As in Fig. 8, but for enlarged and contrast-enhanced photographs of (top) fractured ice pellets and (bottom) outlines. Solid lines in the outline depict silhouette and fracture points (cracks and voids) and dashed lines depict peripheries of bubbles.

1971; Pruppacher and Klett 1997). Thus, ice pellets that freeze rapidly form an ice shell at the surface, and the inner pressure increases as freezing proceeds, because of the inclusion of dissolved air (Dorsey 1948; Blanchard 1951). Rapidly growing ice shells tend to be round in shape and can fracture. Takahashi (1975) demonstrated that fracturing (shattering) occurred when the surface temperature of freezing particles was less than −4°C. This temperature is similar to the simulated minimum particle temperatures in our study. Given the round surfaces and fracturing characteristics, and the inferred sufficient supercooling (−4°C) in this study, slow-falling ice pellets were assumed to form through rapid freezing upon contact with a small number of ice nuclei.

In contrast, fast-falling pellets likely froze more slowly with a relatively smaller supercooling than did the slow-falling pellets. As Yang and Good (1966) noted, water molecules cannot absorb all of the latent heat released during the freezing process when the temperature of supercooled water exceeds −4°C. Slow freezing may account for the formation of ice pellets whose interiors were still water. Additionally, particles with small supercooling have nonuniform freezing speeds biased toward the upstream side of the particles, which is more ventilated than the downstream side, and the unequal inner pressure resulting from nonuniform freezing prevents the formation of cracks (Pruppacher and Schlamp 1975). The slightly deformed surface itself is thought to be indicative of slow and unequal freezing under small supercooling.

4) NUMBER CONCENTRATION FLUX OF SLOW- AND FAST-FALLING ICE PELLETS

Figure 16a illustrates time series of the particle number flux from sedimentation (every 5-s data with a 75-s moving average) of the two groups, limiting the size range from 1.5 to 2.0 mm. The temporal trends exhibited by the two groups were similar, with a correlation coefficient of 0.77, during this ice-pellet event. This result suggests that the two groups fell from the same precipitating cloud and formed from the same group of supercooled raindrops. The highest correlation coefficient between the time series of number flux of the fast-falling group and those of the slow-falling group for the entire period was obtained for no time lag. However, the two groups sometimes exhibited clear temporal phase differences in terms of the peak number fluxes (Figs. 16b–f). For example, the time lags at A–A′, B–B′, C–C′, F–F′, H–H′, L–L′, M–M′, N–N′, O–O′, P–P′, and Q–Q′ ranged from 60 to 160 s. The fluxes of the fast-falling

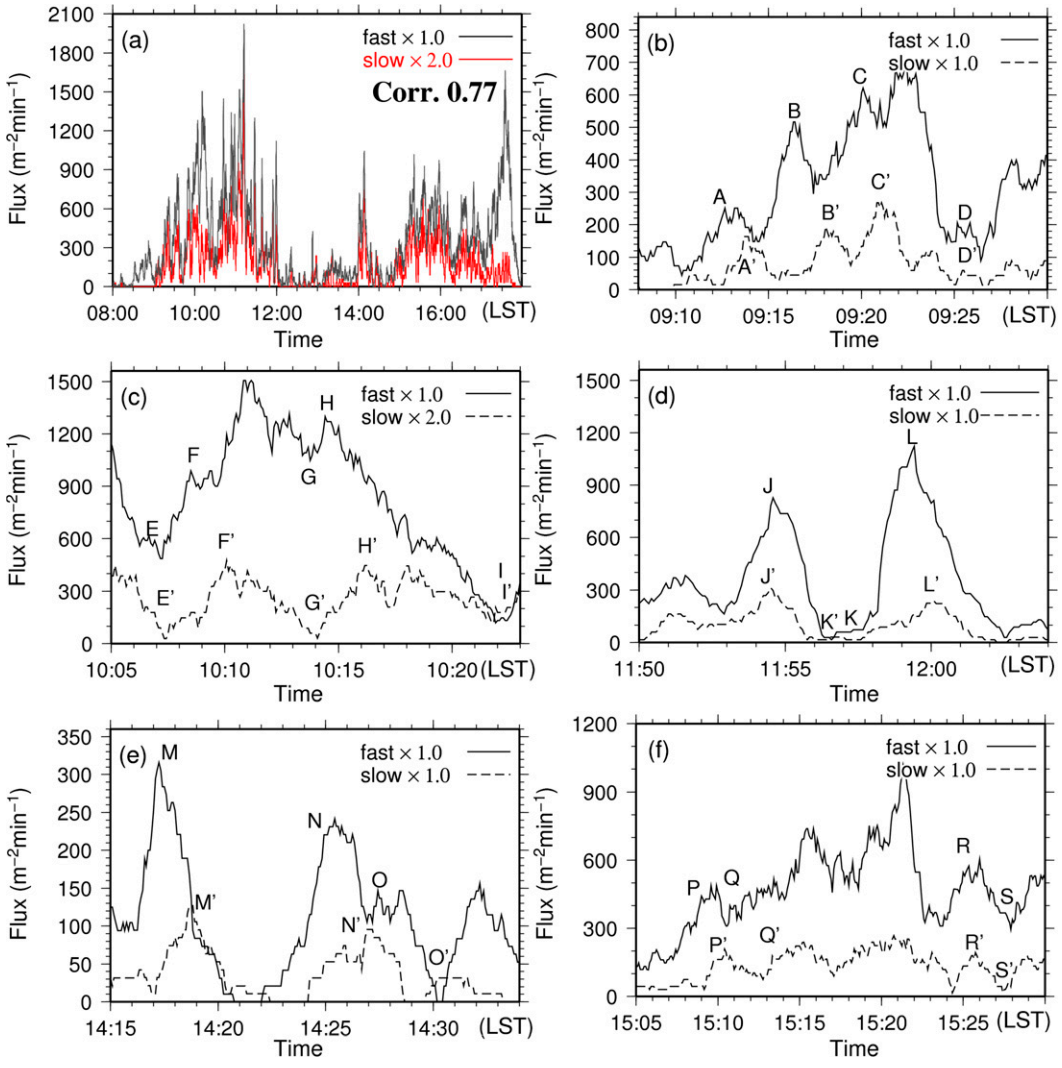

FIG. 16. Time series of particle number concentration fluxes ($m^{-2}\,min^{-1}$) of both fast- and slow-falling groups in the size range of 1.5–2.0 mm. Time resolutions are 5 s with a 75-s moving average for (a) the entire period of the ice-pellet event, (b) 0908–0930, (c) 1005–1023, (d) 1150–1204, (e) 1415–1434, and (f) 1505–1530 LST 10 Apr 2005. A–S indicate local peaks of fast-falling pellets, and A′–S′ indicate local peaks of slow-falling pellets.

group peaked earlier than those of the slow-falling group, especially at the beginning of the period.

We estimated the altitude (air temperature) at which these lags occurred using average falling speeds and lags. Precipitation particles were assumed to form within a horizontally uniform layer cloud associated with a warm front. The average fall velocity of fast-falling particles with diameters of 1.5–2.0 mm was 5.0 m s^{-1} (Fig. 9), whereas that of slow-falling particles was 1.2 m s^{-1}. Thus, the difference in average fall speed was 3.8 m s^{-1}. Estimation of the largest time lag of 160 s at O–O′ suggests an altitude of 608 m with respect to slow-falling ice-particle formation. The altitude corresponds to the minimum wet-bulb temperature (Figs. 10 and 12). This estimation is consistent with the previous discussion [section 4b(3)]: fast-freezing and slow-falling ice pellets formed at wet-bulb temperatures below −4°C. However, a lag shorter than 160 s implies formation at lower altitudes than that of the minimum wet-bulb temperature, and the time lags were quite short in the late stage of each precipitation event. There remain uncertainties; however, it is speculated that slow-falling ice pellets occurred less frequently in the late stage of each precipitation event, because late periods are assumed to increase wet-bulb temperature by evaporation of preceding precipitation as proposed in section 4b(3). Thus, the remaining smaller supercooled raindrops above −4°C would end as fast-falling ice pellets through slow-freezing contacting with ice

crystals/splinters mainly ejected from the preceding slow-falling ice pellets.

5. Conclusions

An ice-pellet event during an unusually warm storm occurred in Sapporo, Japan, on 10 April 2005, and lasted 10 h. The 2DVD observations indicated the simultaneous presence of ice pellets with a bimodal terminal velocity distribution (i.e., fast- and slow-falling velocity groups). We verified ice-pellet formation using observational data and one-dimensional model simulations of melting snowflakes and cooling raindrops, maintained in the supercooled state. We also analyzed the geometrical characteristics of ice pellets for the two fall velocity groups and determined the relationship between particle properties and fall velocities.

One-dimensional model simulations indicated that evaporative cooling of raindrops plays an important role in the formation of ice pellets. Radar observations and several simulations indicated complete melting of snowflakes aloft and persistent supercooling of raindrops by evaporation. Particle temperature was found to be sensitive to environmental temperature and relative humidity, and corresponded to wet-bulb temperatures. The wet-bulb temperature enabled us to clarify the possibility of ice-pellet formation based on both diagnostic and microphysical interpretations. It is likely that contact freezing was the nucleation mechanism at the minimum wet-bulb (particle) temperature altitude of −4°C. Although particle temperatures below −5°C were simulated under the assumption of dry air inflow from a drier nonprecipitating region, the number of ice pellets was likely greater than that of general ice nuclei, suggesting that the generation of crystals or ice splinters after the initial ice-forming event was critical.

Of the two fall velocities, slow-falling ice pellets exhibited properties similar to those of dry hailstones. This indicates that these particles were moderate-density ice particles with microscopic-scale rough surfaces. In addition, tumbling motions may have increased the drag of these particles. Most of the slow-falling ice pellets were round. Furthermore, almost all fractured ice pellets were in the slow-falling group. These features suggest that these particles froze rapidly and uniformly in a relatively cold dry layer with a wet-bulb temperature near −4°C. In contrast, the fast-falling ice pellets exhibited the properties of ice particles with a wet smooth surface, suggesting that they froze slowly in a relatively warm (slightly supercooled) layer by contacting ice crystals or splinters generated by preceding slow-falling ice pellets. More advanced remote sensing and in situ observations will be necessary to confirm the freezing mechanisms of supercooled raindrops presented in this paper. Moreover, few cases of long-lasting ice pellets have been reported in extremely dry, warm conditions (Hanesiak and Stewart 1995; Kumjian and Schenkman 2014). Our next paper will present the synoptic-scale structure of an ice-pellet event, focusing on the contribution of long-duration dry air inflow to evaporative cooling.

Acknowledgments. We thank Dr. Takayo Matsuo and Ms. Kyoko Ikeda for their valuable comments and studies, on which the present study was based. This study was partly supported by the Joint Research Program of the Institute of Low Temperature Science, Hokkaido University, Japan.

REFERENCES

Anderson, M. E., L. D. Carey, W. A. Petersen, and K. R. Knupp, 2011: C-band dual-polarimetric radar signatures of hail. *Electron. J. Oper. Meteor.*, **12** (2), 1–30.

Atlas, D., R. C. Srivastava, and R. S. Sekhon, 1973: Doppler radar characteristics of precipitation at vertical incidence. *Rev. Geophys. Space Phys.*, **11**, 1–35, doi:10.1029/RG011i001p00001.

Beard, K. V., 1992: Ice initiation in warm-base convective clouds: An assessment of microphysical mechanisms. *Atmos. Res.*, **28**, 125–152, doi:10.1016/0169-8095(92)90024-5.

Berezinski, N. A., G. V. Stepanov, and V. G. Khorguani, 1988: Ice forming activity of atmospheric aerosol particles of different sizes. *Atmospheric Aerosols and Nucleation*, P. E. Wagner and G. Vali, Eds., Springer, 233–249.

Blanchard, D. C., 1951: A verification of the Bally-Dorsey theory of spicule formation on sleet pellet events. *J. Meteor.*, **8**, 268–269.

——, 1957: The supercooling, freezing and melting of giant waterdrops at terminal velocity in air. *Artificial Stimulation of Rain*, H. K. Weickmann and W. Smith, Eds., Pergamon Press, 233–245.

Bohren, C., and B. Albrecht, 1998: *Atmospheric Thermodynamics.* Oxford University Press, 403 pp.

Bringi, V. N., and V. Chandrasekar, 2001: *Polarimetric Doppler Weather Radar: Principles and Applications*. Cambridge University Press, 636 pp.

Brooks, C., 1920: The nature of sleet and how it is formed. *Mon. Wea. Rev.*, **48**, 69–72, doi:10.1175/1520-0493(1920)48<69b:TNOSAH>2.0.CO;2.

Brownscombe, J. L., and N. S. C. Thorndike, 1968: Freezing and shattering of water droplets in free fall. *Nature*, **220**, 687–689, doi:10.1038/220687a0.

Cortinas, J. V., Jr., 2000: A climatology of freezing rain in the Great Lakes region of North America. *Mon. Wea. Rev.*, **128**, 3574–3588, doi:10.1175/1520-0493(2001)129<3574:ACOFRI>2.0.CO;2.

——, B. C. Bernstein, C. C. Robbins, and J. W. Strapp, 2004: An analysis of freezing rain, freezing drizzle, and ice pellets across the United States and Canada: 1976–90. *Wea. Forecasting*, **19**, 377–390, doi:10.1175/1520-0434(2004)019<0377:AAOFRF>2.0.CO;2.

Crawford, R. W., and R. E. Stewart, 1995: Precipitation type characteristics at the surface in winter storms. *Cold Reg. Sci. Technol.*, **23**, 215–229, doi:10.1016/0165-232X(94)00014-O.

Dorsey, N. E., 1948: The freezing of supercooled water. *Trans. Amer. Philos. Soc.*, **38**, 247–328, doi:10.2307/1005602.

Dye, J. E., and P. V. Hobbs, 1968: The influence of environmental parameters on the freezing and fragmentation of suspended water drops. *J. Atmos. Sci.*, **25**, 82–96, doi:10.1175/1520-0469(1968)025<0082:TIOEPO>2.0.CO;2.

Edwards, G. R., and L. F. Evans, 1971: Mechanism of activation of ice nuclei. *J. Atmos. Sci.*, **28**, 1443–1447, doi:10.1175/1520-0469(1971)028<1443:TMOAOI>2.0.CO;2.

Gao, Y., T. W. Wu, B. D. Chen, J. Wang, and Y. Liu, 2013: A numerical simulation of microphysical structure of cloud associated with the 2008 winter freezing rain over southern China. *J. Meteor. Soc. Japan*, **91**, 101–117, doi:10.2151/jmsj.2013-202.

Gibson, S., and R. E. Stewart, 2007: Observations of ice pellets during a winter storm. *Atmos. Res.*, **85**, 64–76, doi:10.1016/j.atmosres.2006.11.004.

——, ——, and W. Henson, 2009: On the variation of ice pellet characteristics. *J. Geophys. Res.*, **114**, D09207, doi:10.1029/2008JD011260.

Gokhale, N. R., and O. Lewinter, 1971: Microcinematographic studies of contact nucleation. *J. Appl. Meteor.*, **10**, 469–473, doi:10.1175/1520-0450(1971)010<0469:MSOCN>2.0.CO;2.

——, and J. D. Spengler, 1972: Freezing of freely suspended, supercooled water drops by contact nucleation. *J. Appl. Meteor.*, **11**, 157–160, doi:10.1175/1520-0450(1972)011<0157:FOFSSW>2.0.CO;2.

Hanesiak, J. M., and R. E. Stewart, 1995: The mesoscale and microscale structure of a severe ice pellet storm. *Mon. Wea. Rev.*, **123**, 3144–3162, doi:10.1175/1520-0493(1995)123<3144:TMAMSO>2.0.CO;2.

Heymsfield, A., and R. Wright, 2014: Graupel and hail terminal velocities: Does a ''supercritical'' Reynolds number apply? *J. Atmos. Soc.*, **71**, 3392–3403, doi:10.1175/JAS-D-14-0034.1.

Johnson, D. A., and J. Hallett, 1968: Freezing and shattering of supercooled water drops. *Quart. J. Roy. Meteor. Soc.*, **94**, 468–482, doi:10.1002/qj.49709440204.

Knight, N. C., and A. E. Heymsfield, 1983: Measurement and interpretation of hailstone density and terminal velocity. *J. Atmos. Sci.*, **40**, 1510–1516, doi:10.1175/1520-0469(1983)040<1510:MAIOHD>2.0.CO;2.

Kumjian, M. R., and A. D. Schenkman, 2014: The curious case of ice pellets over middle Tennessee on 1 March 2014. *J. Oper. Meteor.*, **2**, 209–213, doi:10.15191/nwajom.2014.0217.

——, S. M. Ganson, and A. V. Ryzhkov, 2012: Freezing of raindrops in deep convective updrafts: A microphysical and polarimetric model. *J. Atmos. Soc.*, **69**, 3471–3490, doi:10.1175/JAS-D-12-067.1.

——, A. V. Ryzhkov, J. D. Reeves, and T. J. Schuur, 2013: A dual-polarization radar signature of hydrometeor refreezing in winter storms. *J. Appl. Meteor. Climatol.*, **52**, 2549–2566, doi:10.1175/JAMC-D-12-0311.1.

List, R., and R. S. Schemenauer, 1971: Free-fall behavior of planar snow crystals, conical graupel and small hail. *J. Atmos. Soc.*, **28**, 110–115, doi:10.1175/1520-0469(1971)028<0110:FFBOPS>2.0.CO;2.

Martinez, A. T., 1994: On the evaluation of the wet bulb temperature as a function of dry bulb temperature and relative humidity. *Atmósfera*, **7**, 179–184.

Matsukawa, T., 1923: Frozen rain drops at Sapporo. *J. Meteor. Soc. Japan*, **1**, 95–97.

Matsuo, T., and Y. Sasyo, 1981a: Empirical formula for the melting rate of snowflakes. *J. Meteor. Soc. Japan*, **59**, 1–9.

——, and ——, 1981b: Melting of snowflakes below freezing level in the atmosphere. *J. Meteor. Soc. Japan*, **59**, 10–25.

Matsushita, H., and F. Nishino, 2008: A simple method of discriminating between occurrences of freezing rain and ice pellets in the Kanto plain, Japan. *J. Meteor. Soc. Japan*, **86**, 633–648, doi:10.2151/jmsj.86.633.

Mikhailov, M. D., and A. P. Silva Freire, 2013: The drag coefficient of a sphere: An approximation using Shanks transform. *Powder Technol.*, **237**, 432–435, doi:10.1016/j.powtec.2012.12.033.

Mossop, S. C., R. E. Ruskin, and K. J. Heffernan, 1968: Glaciation of a cumulus at approximately −4 °C. *J. Atmos. Sci.*, **25**, 889–905, doi:10.1175/1520-0469(1968)025<0889:GOACAA>2.0.CO;2.

Pitter, R. L., and H. R. Pruppacher, 1973: A wind tunnel investigation of freezing of small water drops falling at terminal velocity in air. *Quart. J. Roy. Meteor. Soc.*, **99**, 540–550, doi:10.1002/qj.49709942111.

Pruppacher, H. R., 1967: Interpretation of experimentally determined growth rates of ice crystals in supercooled water. *J. Chem. Phys.*, **47**, 1807–1813, doi:10.1063/1.1712169.

——, and R. J. Schlamp, 1975: A wind tunnel investigation on ice multiplication by freezing of waterdrops falling at terminal velocity in air. *J. Geophys. Res.*, **80**, 380–386, doi:10.1029/JC080i003p00380.

——, and J. D. Klett, 1997: *Microphysics of Clouds and Precipitation.* Kluwer Academic, 954 pp.

Rasmussen, R. M., and A. J. Heymsfield, 1987: Melting and shedding of graupel and hail. Part I: Model physics. *J. Atmos. Soc.*, **44**, 2754–2763, doi:10.1175/1520-0469(1987)044<2754:MASOGA>2.0.CO;2.

Ryzhkov, A. V., H. D. Reeves, T. J. Schuur, M. R. Kumjian, and D. S. Zrnic, 2011: Investigations of polarimetric radar signatures in winter storms and their relation to aircraft icing and freezing rain. *Proc. 35th Conf. on Radar Meteorology*, Pittsburgh, PA, Amer. Meteor. Soc., 197. [Available online at https://ams.confex.com/ams/35Radar/webprogram/Paper191245.html.]

Sassen, K., P. J. DeMott, J. M. Prospero, and M. R. Poellot, 2003: Saharan dust storms and indirect aerosol effects on clouds: CRYSTAL-FACE results. *Geophys. Res. Lett.*, **30**, 1633, doi:10.1029/2003GL017371.

Schmitt, C. G., and A. J. Heymsfield, 2014: Observational quantification of the separation of simple and complex atmospheric ice particles. *Geophys. Res. Lett.*, **41**, 1301–1307, doi:10.1002/2013GL058781.

Schönhuber, M., G. Lammer, and W. L. Randeu, 2007: One decade of imaging precipitation measurement by 2d-video-disdrometer. *Adv. Geosci.*, **10**, 85–90, doi:10.5194/adgeo-10-85-2007.

——, ——, and ——, 2008: The 2D-videodisdrometer. precipitation: *Advances in Measurement, Estimation and Prediction*, S. Michaelides, Ed., Springer, 3–31.

Selberg, B. P., and J. A. Nicholls, 1968: Drag coefficient of small spherical particles. *AIAA J.*, **6**, 401–408, doi:10.2514/3.4513.

Spengler, J. D., and N. R. Gokhale, 1972: Freezing of freely suspended supercooled water drops in a large vertical wind tunnel. *J. Appl. Meteor.*, **11**, 1101–1107, doi:10.1175/1520-0450(1972)011<1101:FOFSSW>2.0.CO;2.

Stewart, R. E., and P. King, 1987: Freezing precipitation in winter storms. *Mon. Wea. Rev.*, **115**, 1270–1279, doi:10.1175/1520-0493(1987)115<1270:FPIWS>2.0.CO;2.

——, and R. W. Crawford, 1995: Some characteristics of the precipitation formed within winter storms over eastern Newfoundland. *Atmos. Res.*, **36**, 17–37, doi:10.1016/0169-8095(94)00004-W.

Straka, J. M., 2009: *Cloud and Precipitation Microphysics.* Cambridge University Press, 406 pp.

Takahashi, C., 1975: Deformation of frozen drops and their frequencies. *J. Meteor. Soc. Japan*, **53**, 402–411.

——, and A. Yamashita, 1969: Deformation and fragmentation of freezing water drops in free fall. *J. Meteor. Soc. Japan*, **47**, 431–436.

——, and ——, 1970: Shattering of frozen water drops in a supercooled cloud. *J. Meteor. Soc. Japan*, **48**, 373–376.

Thériault, J. M., and R. E. Stewart, 2010: A parameterization of the microphysical processes forming many types of winter precipitation. *J. Atmos. Sci.*, **67**, 1492–1508, doi:10.1175/2009JAS3224.1.

Watts, R. G., 1971: Relaxation time and steady evaporation rate of freely falling raindrops. *J. Atmos. Sci.*, **28**, 219–225, doi:10.1175/1520-0469(1971)028<0219:RTASER>2.0.CO;2.

Yang, L. C., and W. B. Good, 1966: Crystallization rate of supercooled water in cylindrical tubes. *J. Geophys. Res.*, **71**, 2465–2469, doi:10.1029/JZ071i010p02465.

Zerr, R. J., 1997: Freezing rain: An observational and theoretical study. *J. Appl. Meteor.*, **36**, 1647–1661, doi:10.1175/1520-0450(1997)036<1647:FRAOAT>2.0.CO;2.

Zhang, G., S. Luchs, A. Ryzhkov, M. Xue, L. Ryzhkova, and Q. Cao, 2011: Winter precipitation microphysics characterized by polarimetric radar and video disdrometer observations in central Oklahoma. *J. Appl. Meteor. Climatol.*, **50**, 1558–1570, doi:10.1175/2011JAMC2343.1.